RSC Advances

PAPER

View Article Online
View Journal | View Issue

Cite this: *RSC Adv.*, 2015, **5**, 106005

Hydrogel formed by the co-assembly of sodium laurate and silica nanoparticles†

Ying Wei,[a] Yijie Wang,[a] Congrui Wei,[a] Qiang Zhao,[a] Yun Yan,[a] Jiang Yang*[b] and Jianbin Huang*[a]

Received 9th November 2015
Accepted 8th December 2015

DOI: 10.1039/c5ra23636c

www.rsc.org/advances

Co-assembly between surfactants and inorganic nanoparticles is an appealing research field which has been proved to be an effective approach to create hybrid materials. In this paper, a new type of co-assembled hydrogel formed by an anionic surfactant and nanoparticles is reported. The hydrogel can be achieved by mixing the anionic surfactant, sodium laurate (SL), with silica nanoparticles (silica NPs) in an aqueous solution with dissolved potassium chloride (KCl). It was found that the silica NPs and SL co-assembled to intertwined 1D fibers as well as a macroscopic hydrogel, where the complexes of amphiphilic molecules and nanoparticles acted as building blocks. We proved that the formation of the hydrogels originates from the hydrogen bond and hydrophobic effect in the SL and silica NPs co-assembled system. In addition, the silica NPs assembled with SL molecules by hydrogen bonds, rather than SL aggregates, which is different with the conventional studies. The novel phenomenon of co-assembly between a surfactant and nanoparticles not only provides a new strategy for the construction of co-assemblies, but also may advance a better understanding of the fundamental science.

Introduction

Amphiphilic molecules are particularly promising self-assembled tools due to their controllable molecular structures and stimuli-responsive properties.[1–3] The assembly of amphiphilic molecules with inorganic nanoparticles,[4–6] integrating multiple functional components for synergistic properties,[7,8] plays an important role in chemistry, biology and materials science.[9,10] However, compared with the numerous studies on amphiphiles and nanoparticles, research of the co-assembly of amphiphilic molecules and nanoparticles is rarely reported.[11] This usually required the synthesis of grafted nanoparticles using amphiphilic molecules.[12,13] These conventional strategies are irreversible and require complicated molecular designs, which greatly limit the wide application of these aggregates in materials science.[14,15] Thus, the co-assembly of amphiphilic molecules and unmodified nanoparticles provides a feasible approach by bottom-up strategy. In the co-assembly systems based on amphiphiles and nanoparticles, the main challenge remains to choose suitable and controlled building blocks, in terms of size and structure. In contrast with 'static' and hard nanoparticles, these amphiphilic aggregates are intrinsically self-assembled, soft and 'dynamic', undergoing reversible assembly and disassembly.[16] On the other hand, the interactions between surfactant monomers and nanoparticles, aggregates and nanoparticles are indistinct and complicated. Thus, it is of great significance to investigate the co-assembled systems based on amphiphilic molecules and unmodified nanoparticles.

However, most of the limited research on the co-assembly of unmodified nanoparticles and amphiphiles in solution focused mostly on the systems which the nanoparticles interact with surfactant aggregates, such as wormlike micelles (WLMs)[17] and lamellar phases.[18] For instance, Norman and co-workers[19] had shown that silica nanoparticles added into the system of cetyltrimethyl ammonium bromide CTAB/$NaNO_3$ WLMs resulted in a so-called "double network" in which the nanoparticles supplement the inherent viscoelasticity of entangled WLMs acting as physical cross-links between micelles. To our knowledge, the co-assembly of amphiphilic molecules and unmodified nanoparticles, where the complexes of amphiphilic molecules and nanoparticles act as building blocks in aggregates, have rarely reported. Thus, the fabrication of the novel co-assemblies utilizing amphiphilic molecules and unmodified nanoparticles will be of topical interest and great importance, which is beneficial to investigate the interactions between nanoparticles and surfactant molecules.

To carry out the novel co-assembly systems where the complexes of amphiphilic molecules and nanoparticles act as building blocks, we combined anionic surfactant, sodium fatty

[a]*Beijing National Laboratory for Molecular Sciences (BNLMS), State Key Laboratory for Structural Chemistry of Unstable and Stable Species, College of Chemistry and Molecular Engineering, Peking University, Beijing 100871, China. E-mail: jbhuang@pku.edu.cn*

[b]*Department of Petroleum Engineering, Xi'an Petroleum University, Xi'an, Shaanxi 710065, China. E-mail: jyang@xsyu.edu.cn*

† Electronic supplementary information (ESI) available. See DOI: 10.1039/c5ra23636c

acid with carboxylic ion, with silica nanoparticles (silica NPs) to realize the proposition. The results showed that the sodium laurate and silica NPs spontaneously co-assembled into well-defined fibers, accompanied by hydrogel formation, at the concentration of 50 mM SL, 3 wt% silica NPs and 400 mM KCl, whereas the mixed system of sodium laurate and KCl failed to form hydrogel. From the results of TEM, DLS and FT-IR spectrum, the origins of the one-dimensional nanostructure will be proposed based on hydrogen bond and hydrophobic force in SL and silica NPs systems. Intriguingly, the silica NPs and SL molecules first co-assembled to clusters and then "glue" together like "necklace" into fibers under excess SL molecules. It was also found that the Si–OH on the surface of silica NPs was essential in the co-assemblies. The effect of KCl salt concentration on the co-assembly system is also investigated. It is anticipated that this study can help to understand the mechanism of the co-assemblies, and contribute to help build hierarchical assembly of nanoparticles and surfactants systems.

Experimental

Materials

The anionic surfactant sodium laurate (SL) (Fig. 1a) and potassium chloride (KCl) were products of C.P. grade from Sinopharm Chemical Reagent Co., Ltd and were used without further purification. Silica nanoparticles (silica NPs) as a liquid dispersion used in this research was purchased from Nanjing Haitai Nano Materials Company. The silica nanoparticles, which have silanol (Si–OH) groups (Fig. 1b) on its particle surfaces, are 30 nm in diameter with negative charged surface. Other compounds (A.R. grade) were used as received. Distilled water was purified through Milli-Q Advantage A10 Ultrapure Water System.

Samples preparation

Concentrated solution of sodium laurate was prepared in the distilled water. Aqueous stock solutions of other materials were also prepared in the distilled water. The samples were prepared by simply mixing silica nanoparticles (silica NPs) solution, sodium laurate solution (SL) and potassium chloride (KCl) solution in a test tube. The samples were vortex mixed and equilibrated at 25 °C in a thermostat at least for two days before further analyses. During this period, a self-supporting hydrogel can form. All the samples were studied at 25 °C unless specified.

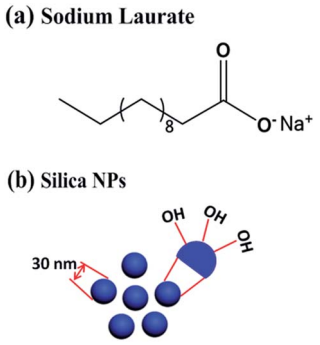

Fig. 1 The main components of the hydrogel described in this paper (a) molecular structure of sodium laurate; and (b) silica nanoparticles. The diameter of silica NPs is about 30 nm. The silica with a negative surface is covered silanol (Si–OH) groups.

Rheological measurements

The rheological properties of samples were measured with a ThermoHaake RS300 rheometer (cone and plate geometry of 35 mm in diameter with the cone gap equal to 0.100 mm). The temperature was controlled at 25 ± 0.05 °C. A solvent trap was used to avoid water evaporation. Frequency spectra were recorded in the linear viscoelastic regime of the samples determined from dynamic strain sweep measurements. Dynamic stress sweeps were carried out at a fix frequency of 1 Hz. The zero-shear viscosity η_0 of the sample was determined from controlled stress measurement by extrapolating the viscosity-shear stress curve to zero shear-rate.

Transmission electron microscopy (TEM)

A Tecnai G2 F20 TEM (120 kV) was employed to observe the morphology of assemblies. Drops of samples were put onto 230 mesh copper grids coated with a Formvar film. Excess water was removed by filter paper, and the samples were placed at room temperature to dry before TEM observation.

Fourier transform infrared (FT-IR)

The Fourier transform infrared spectrum were recorded on a Nicolet iN10 MX infrared spectrometer (Thermo Scientific Co., America). The samples were frozen in liquid nitrogen and subsequently lyophilized for 48 h before FT-IR measurements.

Dynamic light scattering (DLS)

Dynamic light scattering (DLS) measurements were performed with a spectrometer (ALV-5000/E/WIN Multiple Tau Digital Correlator) and a Spectra-Physics 2017 200 mW Ar laser (632.8 nm wavelength) at the scattering angle 90°. The samples were filtered with 450 nm filters.

Results and discussion

In our study of the co-assemblies, spherical silica particles at 30 nm-diameter with weak negative charged surface (−20 mV) were used. When the silica NPs are mixed with anionic surfactant, sodium laurate, the sample is semitransparent fluid with opalescence due to the weak electronic repulsion between SL and silica NPs at 25 °C (Fig. S1a†). In comparison, cationic surfactant, cetyltrimethyl ammonium bromide (CTAB), is also mixed with silica NPs solution. Due to the electrostatic attraction between CTAB and silica NPs, the silica NPs agglomerate into precipitates (Fig. S1b†). Thus, we chose anionic surfactant, sodium laurate, as one of the co-assembled building blocks for further investigation.

Hydrogel formed by SL–silica NPs co-assembly

Here we attempted to use KCl salt to screen the weak electrostatic repulsion between SL molecules and silica NPs. It has been proved that the SL molecules with excess KCl systems could not form hydrogels at any concentration.[20] Upon addition of 100 mM KCl, the hydrogel was obtained by simply mixing stock solution of SL and silica NPs. Fig. 2 showed the phase diagram of the SL–silica NPs systems at the fixed 100 mM KCl concentration. Intriguingly, the hydrogel can be obtained at low concentration of 5 mM sodium laurate. The key factor for preparation of these hydrogels was the appropriate silica NPs concentration, 2 wt%. In addition, rapid gelation could be observed by the increasing concentration of KCl. At concentration of 400 mM KCl, the hydrogelation ability was studied by an inverted test tube method (Table 1). It can be found that the gelation time can be significantly decreased when the concentration of SL–silica NPs co-assembly system was increased. To gain insight into the microstructure and gelation mechanism of the co-assembled hydrogels, 50 mM SL–400 mM KCl systems were chosen as the model for further studies.

The rheological properties of the SL–silica NPs systems were measured by static and dynamic rheology. The viscosity η_0 of the 50 mM SL–400 mM KCl solution is about 0.1 Pa s. As the concentration of silica NPs increased to 1 wt%, the zero-shear viscosity η_0 of the sample shows a dramatic growth about 3000 Pa s (Fig. S2a†), which is nearly 10^4 fold enhancement. The sharply increasing of viscosity suggests the co-assembly between SL–silica NPs. To confirm this hypothesis, upon adding TiO_2 NPs to 50 mM SL solution, the improvement of viscosity of system is not obvious (Fig. S2b†). The viscosities of the mixed system are increased as the silica NPs concentration increased (Fig. S2a†). All these samples exhibit a viscosity plateau under low shear-stresses and shear-thinning properties at high shear-stresses. As demonstrated in Fig. 3a, for the concentration of silica NPs at 0 and 1 wt%, both G' and G'' were strong functions of frequency. For the silica NPs concentration at 2 wt%, the sample had been obviously changed, both elastic modulus G' and viscous modulus G'' remain at a plateau over the investigated oscillating frequency. Also, the values of G' are about an order of magnitude greater than G'' for all samples. This is a typical solidlike behavior of a hydrogel.[21] On the other hand, when the silica NPs concentration is increased, the hydrogel mechanical strength can be greatly improved, as shown in Fig. 3b. For example, as the silica NPs increases to 5 wt%, the yield stress of the sample is up to 40 Pa.

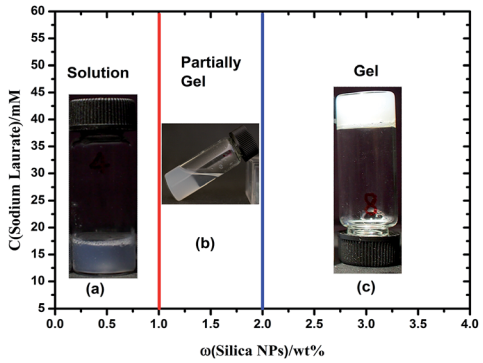

Fig. 2 The phase diagram for the SL–silica NPs co-assembly system at the fixed 100 mM KCl concentration. The insets show macroscopic photos of the 50 mM SL–100 mM KCl samples with different concentration of silica NPs, (a) 0.5 wt% solution, (b) 1 wt% partially gel and (c) 2 wt% gel.

Table 1 Gelation test of sodium laurate/silica nanoparticles system at the concentration of 400 mM KCl at 25 °C[a]

SL/mM	Silica NPs/wt%	Property	Gel time
5	1.0	PG	—
5	2.0	G	1 d
10	1.0	PG	—
10	2.0	G	10 h
50	1.0	PG	—
50	2.0	G	3 h
50	3.0	G	1 h

[a] G: gel; PG: partially gel; S: solution; d: day(s); h: hour(s).

Co-assembled nanostructures of the SL–KCl–silica NPs hydrogel

We first carried out transmission electronic microscopy (TEM) to obtain a direct view of the morphology of the SL–KCl–silica NPs hydrogel. As shown in Fig. 4, the TEM image revealed that

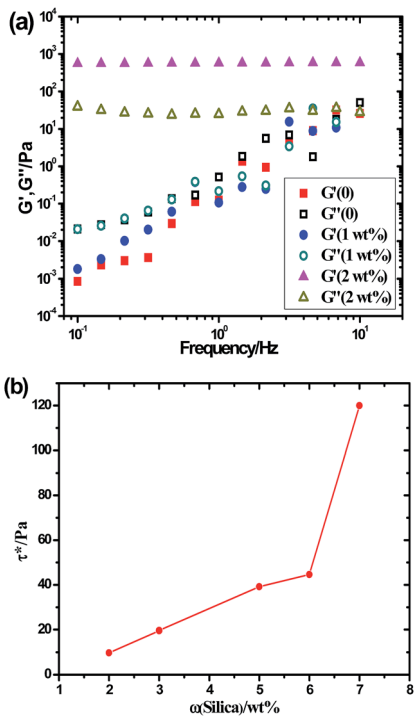

Fig. 3 (a) Dynamic rheological frequency sweep of 50 mM SL–400 mM KCl with added 0, 1 wt%, 2 wt% silica NPs respectively. The solid symbols are donated to storage modulus G', and the open symbols are to loss storage modulus G''. (b) The yield stress as a function of silica NPs concentration for the 50 mM SL–400 mM KCl systems.

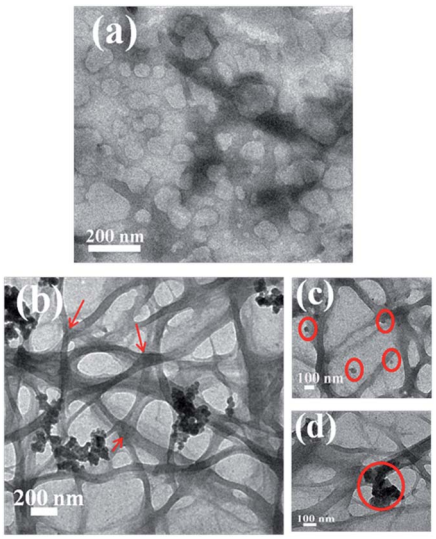

Fig. 4 (a) Negative-staining TEM image of nanostructure in the system of 50 mM SL–400 mM KCl solution. (b–d) TEM images of co-assembled nanostructures in the system of 50 mM SL–400 mM KCl–3 wt% silica NPs, and silica NPs can be obviously found in the red circles in the images (c) and (d); the red arrow clearly indicates the entanglement fibers.

the 50 mM SL–400 mM KCl–3 wt% silica NPs sample was composed of intertwined fibers (Fig. 4b–d), whereas the 50 mM SL–400 mM KCl system stained by uranyl acetate was vesicles (Fig. 4a), indicating that the interwoven networks were formed by the co-assembly of SL and silica NPs. The co-assembled fibers were 50–100 nm in width and a few micrometers in length. These 1D nanofibers further overlaped and entangled into a 3D network, which may be responsible for the robustness of the co-assembled hydrogel. It should be mentioned that the incorporation of silica NPs can provide enough contrast toward an electron beam. Consequently, the SL–KCl–silica NPs fibers can be directly observed under TEM without staining, and this can further confirm that the silica NPs were a part of the co-assembled fibers. In addition, an enlarged image of TEM indicated that the silica NPs aggregations also act as physical cross-links between the fibers (Fig. 4d). Moreover, it is possible that with the concentration of silica NPs increasing in the systems, the structures of the co-assembled nanofibers become harder to disrupt *via* shear. This may explain the higher yield stress. These results were attributed to the interactions between SL and silica NPs.

Mechanism of the SL–silica NPs co-assembly

Further experiments were performed to explore the structural origin of the SL–silica NPs–KCl co-assembly. Fourier transform infrared (FT-IR) spectroscopy of silica NPs in solid state and the co-assembled hydrogel state provides important information about the hydrogen bonds between SL molecules and silica NPs (Fig. 5). Upon the addition of 5 mM SL into the silica NPs solution, the hydroxyl peak of co-assembled system appears at the lower wavenumber of 3374 cm^{-1}, whereas that for the

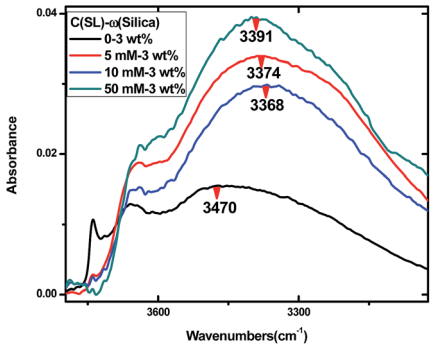

Fig. 5 *In situ* FT-IR spectra of the co-assembled systems at 0 (dark line), 5 mM (red line), 10 mM (blue line) and 50 mM (green line) SL at a fixed concentration of 400 mM KCl and 3 wt% silica NPs.

hydroxyl peak of silica NPs occurs at 3470 cm^{-1}, suggesting the formation of strong hydrogen bonding.[22] This is due to the headgroup COO^- of SL molecules easily forming hydrogen bond with Si–OH. This important role of hydrogen bond between silica NPs and SL can be also demonstrated by replacing SL with sodium dodecyl sulfate, in which one-dimensional fibers and hydrogel cannot be observed (Fig. S3a†). In addition, it was found that when SL was replaced by undecylenic acid, which is similar in structure with head group COO^-, hydrogel can also obtained (Fig. S3b†). These results further indicated the indispensable role of COO^-–Si–OH hydrogen bond.

To obtain further insight into the nanostructures for the SL–silica NPs–KCl co-assembly, the influence of the SL concentration varied from 5 mM to 50 mM was investigated by rheological measurements at the concentration of 400 mM KCl and 3 wt% silica NPs. As shown in Fig. 6, with the variation concentration of SL, the SL–silica NPs–KCl co-assembly systems are divided into two regions in accordance with the viscosities. In region I, the zero-shear viscosities remain high at low concentration, and then dramatically decrease at 15 mM. In region II, from 15 mM to 50 mM, the zero-shear viscosities increase gradually and at high surfactant concentration, they almost remain at a plateau value. Hence, with the variation of the SL concentration, it is

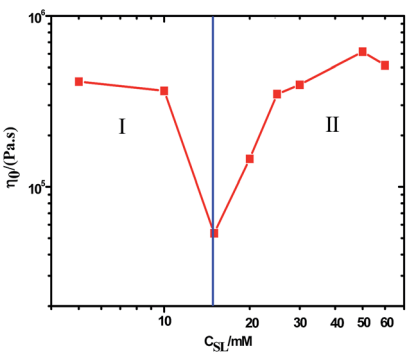

Fig. 6 The zero-shear viscosity η_0 as a function of SL concentration while keeping the salt KCl and silica NPs concentration at 400 mM and 3 wt% respectively.

obvious that the nanostructures of the co-assembled systems in different regions are remarkably different as will be demonstrated by TEM. As shown in Fig. 7, the morphological evolution is closely related to the variation of SL concentration, which was in agreement with the variation of the zero-shear viscosities in the co-assembly systems. It can find that the dispersed silica NPs (Fig. S4†) aggregated into clusters, with the size of clusters decreasing upon SL concentration increasing from 5 mM to 15 mM (Fig. 7a and b), which was responsible for the zero-shear viscosities dramatically decreasing in region I. In region II, with the SL concentration reaching 20 mM, due to the hydrophobic effect, the silica NPs clusters begin to connect with each other, demonstrated by Fig. 7c–f. As the SL concentration reaches 50 mM, the silica NPs and SL molecules are co-assemble to fibrils. Additionally, when the concentration of SL reached to 50 mM, the OH vibration appears at 3391 cm^{-1}, while the OH vibration of 10 mM SL occurs at 3368 cm^{-1} (Fig. 5). It suggests that the excess SL molecules destroyed the hydrogen bonds between the two components. Moreover, with the increasing concentration of SL, the hydrophobic force increased accordingly. Consequently, the SL–silica NPs co-assembled nanofibers were formed by the synergic effect of multiple noncovalent interactions.

From above experimental results, a scheme of the evolution of the SL–silica NPs co-assemblies is proposed in Scheme 1. Owing to the hydrogen bond and hydrophobic effect in the SL–silica NPs system, at lower concentration of SL molecules, the silica NPs first assembled with SL, and then aggregated into clusters (Scheme 1a). Upon the increasing of the concentration of SL, the co-assembled silica NPs "glue" together into well-defined fibers (Scheme 1b), where the hydrophobic effect plays a leading role in the system.

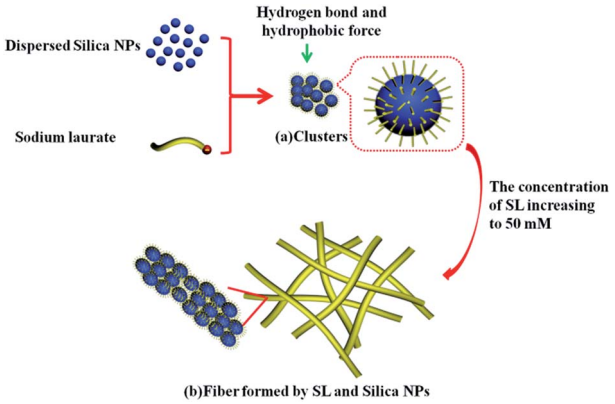

Scheme 1 The schematic aggregate morphology transition of the SL–silica NPs co-assembled systems with the SL increasing at the concentration of 400 mM KCl and 3 wt% silica NPs.

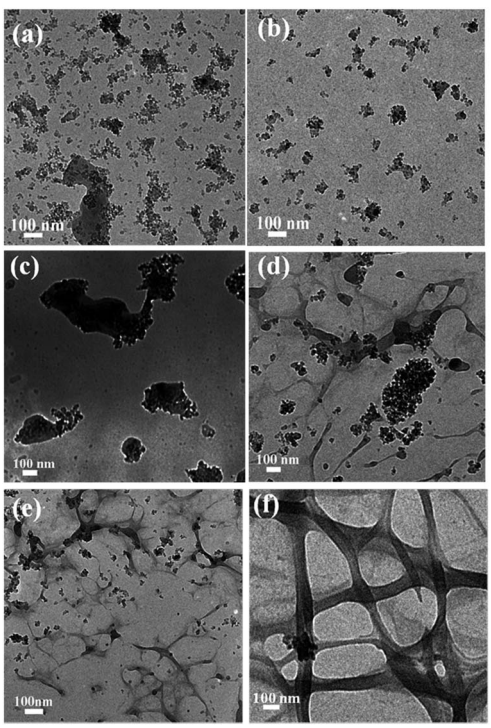

Fig. 7 TEM images of the mixed systems which vary the concentration of SL from 5 mM to 50 mM at 400 mM KCl and 3 wt% silica NPs. (a) 5 mM, (b) 15 mM, (c) 20 mM, (d) 25 mM, (e) 40 mM, (f) 50 mM.

The effect of salt concentration in the co-assembly systems

For many surfactant systems, it has observed that the zero-shear viscosity increases with salt concentration, reaching a maximum and then decreasing at high ionic strength.[23] This behavior was also observed in the hybrid hydrogels at different KCl concentration, as shown in Fig. 8. Without the KCl, the systems of different SL concentrations and silica NPs failed to form hydrogel. It suggested that the salt KCl act as an indispensable role in the co-assembly systems. Upon the KCl concentration varied from 100 to 800 mM, the zero-shear viscosities reached a maximum and then decreased at the concentration of 50 mM SL and 3 wt% silica NPs (Fig. 8). The increased zero-shear viscosities have been interpreted as potassium ions can decrease electrostatic repulsion between carboxyl head groups,[24] which will promote the aggregate of the two building blocks. In addition, it can weak the electrostatic repulsion between silica nanoparticles, which had been further demonstrated by ζ-potential (Table S1†). Consequently, the screening effect of the KCl lead to larger aggregates, resulting in the formation of fibers, as shown in Fig. 9a and b. With the increases of the concentration of KCl to 200 mM, we can observe

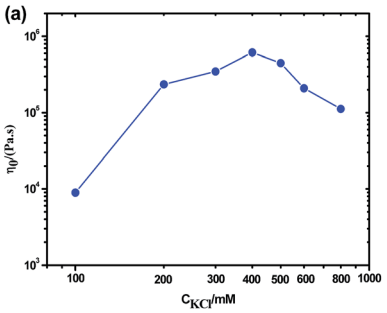

Fig. 8 The zero-shear viscosity as a function of concentration of KCl for the 50 mM SL–3 wt% silica NPs systems.

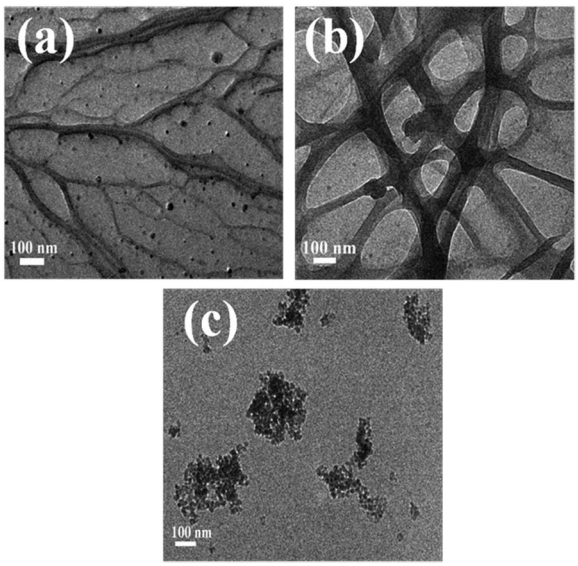

Fig. 9 TEM images of SL–silica NPs–KCl co-assembly systems at 50 mM SL–3 wt% silica NPs with different KCl concentration, (a) 200 mM, (b) 400 mM and (c) 600 mM.

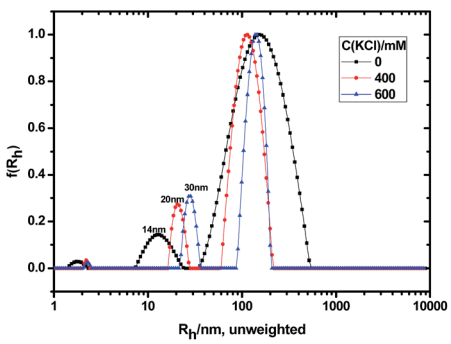

Fig. 10 Hydrodynamic radius (R_h) distributions for the samples of 1 wt% silica NPs with different concentration of KCl 0 mM (black line), 400 mM (red line) and 600 mM (blue line).

the coexistence of fibrils and silica NPs, while the system assembles to uniform fibrils containing SL molecules and silica NPs at the concentration of 400 mM, which accounts for the improvement of mechanical properties. Upon the concentration of KCl above 400 mM, the nanoparticles are conglomerate, which has been also examined by light-scattering measurements (Fig. 10). The diameter of silica NPs reached to 60 nm at the concentration of 600 mM KCl. As a consequence, a large number of SL molecules were adsorbed to conglomerate nanoparticles which destroyed the nanofibers (Fig. 9c), accompanied by the decreasing zero-shear viscosity (Fig. 8). The behaviour is similar in different concentrations of SL 5 mM, 10 mM and 25 mM with 3 wt% silica NPs at different concentration of KCl (Fig. S5†).

Conclusion

In conclusion, we have demonstrated that the co-assembly between SL and silica NPs with the aid of KCl provided a facile method for the hydrogel fabrication. A distinct co-assembly hydrogel arising from the entanglement of 1D nanofibers was obtained. The silica NPs were not connected to the network structures, but assembled to nanofibers with SL molecules with the aid of KCl. The complexes of amphiphilic molecules and nanoparticles acted as building blocks in the aggregates. Hydrogen bond and hydrophobic effect accounted for the hydrogel formation and the co-assemblies in SL–silica NPs–KCl systems. As opposed to conventional surfactant-nanoparticles studies, the most notable feature of our systems is that the silica NPs combined with SL molecules, rather than the aggregates, can co-assemble to fibers. Such a unique phenomenon of the nanostructures provides the new insight of the nanoparticles-surfactant co-assembly systems and its applications in industry.

Acknowledgements

This work was supported by the National Natural Science Foundation of China (Grant No. 21473005, 51174163), the National Basic Research Program of China (973 Program, 2013CB933800).

References

1 A. Das and S. Ghosh, *Angew. Chem.*, 2014, **126**, 1110–1115.
2 K. Matsuurua, *RSC Adv.*, 2014, **4**, 2942–2953.
3 B. G. Bag and R. Majumdar, *RSC Adv.*, 2012, **2**, 8623–8626.
4 B. Zhang, W. Zhao and D. Wang, *Chem. Sci.*, 2012, **3**, 2252–2256.
5 Y. Yan, H. Wang, B. Li, G. Hou, Z. Yin, L. Wu and V. W. Yam, *Angew. Chem.*, 2010, **122**, 9419–9422.
6 S. Rose, A. Prevoteau, P. Elzière, D. Hourdet, A. Marcellan and L. Leibler, *Nature*, 2014, **505**, 382–385.
7 J. C. MacDonald and G. M. Whitesides, *Chem. Rev.*, 1994, **94**, 2383–2420.
8 J. M. Lehn, *Angew. Chem., Int. Ed. Engl.*, 1990, **29**, 1304–1319.
9 P. Ilg, *Soft Matter*, 2013, **9**, 3465–3468.
10 V. P. Torchilin, *Nat. Rev. Drug Discovery*, 2014, **13**, 813–827.
11 Q. Yao, X. Yuan, Y. Yu, Y. Yu, J. Xie and J. Y. Lee, *J. Am. Chem. Soc.*, 2015, **137**, 2128–2136.
12 T. Bian, L. Shang, H. Yu, M. T. Perez, L. Z. Wu, C. H. Tung, Z. Nie, Z. Tang and T. Zhang, *Adv. Mater.*, 2014, **26**, 5613–5618.
13 P. K. Kundu, D. Samanta, R. Leizrowice, B. Margulis, H. Zhao, M. Börner, T. Udayabhaskararao, D. Manna and R. Klajn, *Nat. Chem.*, 2015, **7**, 646–652.
14 S. Bhattacharya, A. Srivastava and A. Pal, *Angew. Chem.*, 2006, **118**, 3000–3003.
15 B. Adhikari and A. Banerjee, *Chem.–Eur. J.*, 2010, **16**, 13698–13705.
16 V. Degiorgio and M. Corti, *Physics of Amphiphiles–micelles, Vesicles, and Microemulsions*, North Holland, 1985, pp. 19–29, 1983: Varenna on Lake Como, July 1983, Villa Monastero.
17 M. E. Helgeson, T. K. Hodgdon, E. W. Kaler, N. J. Wagner, M. Vethamuthu and K. Ananthapadmanabhan, *Langmuir*, 2010, **26**, 8049–8060.

18 G. Salamat and E. W. Kaler, *Langmuir*, 1999, **15**, 5414–5421.
19 M. E. Helgeson, T. K. Hodgdon, E. W. Kaler and N. J. Wagner, *J. Colloid Interface Sci.*, 2010, **349**, 1–12.
20 Z. Yuan, W. Lu, W. Liu and J. Hao, *Soft Matter*, 2008, **4**, 1639–1644.
21 R. G. Weiss, *Langmuir*, 2009, **25**, 8369.
22 P. Akcora, H. Liu, S. K. Kumar, J. Moll, Y. Li, B. C. Benicewicz, L. S. Schadler, D. Acehan, A. Z. Panagiotopoulos and V. Pryamitsyn, *Nat. Mater.*, 2009, **8**, 354–359.
23 S. R. Raghavan, H. Edlund and E. W. Kaler, *Langmuir*, 2002, **18**, 1056–1064.
24 Y. Lin, Y. Qiao, P. Tang, Z. Li and J. Huang, *Soft Matter*, 2011, **7**, 2762–2769.